Accepted Manuscript


# Monitoring PWM Signals in Stand-Alone Photovoltaic Systems

G. Jiménez-Castillo, F.J Muñoz-Rodríguez, C. Rus-Casas, J.C. Hernández, G.M Tina

PII: S0263-2241(18)31012-1
DOI: https://doi.org/10.1016/j.measurement.2018.10.075
Reference: MEASUR 6015

To appear in: *Measurement*

Received Date: 13 November 2017
Revised Date: 9 October 2018
Accepted Date: 20 October 2018

Please cite this article as: G. Jiménez-Castillo, F.J Muñoz-Rodríguez, C. Rus-Casas, J.C. Hernández, G.M Tina, Monitoring PWM Signals in Stand-Alone Photovoltaic Systems, *Measurement* (2018), doi: https://doi.org/10.1016/j.measurement.2018.10.075

This is a PDF file of an unedited manuscript that has been accepted for publication. As a service to our customers we are providing this early version of the manuscript. The manuscript will undergo copyediting, typesetting, and review of the resulting proof before it is published in its final form. Please note that during the production process errors may be discovered which could affect the content, and all legal disclaimers that apply to the journal pertain.

ACCEPTED MANUSCRIPT

# Monitoring PWM Signals in Stand-Alone Photovoltaic Systems.

G. Jiménez-Castillo[(1)], F.J Muñoz-Rodríguez[(1,2)], C. Rus-Casas[(1,2)], J.C. Hernández[(4)] , G.M Tina[(3)]

*[(1)] Department of Electronic and Automatic Engineering, University of Jaén, Campus Lagunillas s/n, Edificio A3, 23071, Jaén, Spain*

*[(2)] Centre of Advanced Studies in Energy and Environment CEAEMA, University of Jaen, Spain*

*[(3)] Department of Electrical, Electronics and Informatics Engineering, University of Catania, Catania, Italy*

*(4) Department of Electrical Engineering, University of Jaén, Campus Lagunillas s/n, Edificio A3, Jaén 23071, Spain*

* Corresponding author. E-mail address: crus@ujaen.es. Tel.: +34 953 21

Abstract

The performance of stand-alone photovoltaic systems (SAPV) can be evaluated by monitoring them in the field using data acquisition systems (DASs). Most SAPV systems use battery charge controllers with pulse width modulation (PWM) to regulate the current into the battery. The PWM signals generated by battery charge controllers imply monitoring challenges due to the complexity of this type of signal. In this sense, the aim of this paper is to develop a new and simple monitoring technique for SAPV systems which can estimate the signals provided by a PWM battery charge controller, thus avoiding expensive DASs, simultaneous sampling and the huge amount of collected data. The estimation of PWM signal parameters, such as the duty factor ($d_f$) or high and low states, shows high accuracy, with the mean absolute percentage error lower than 1.4%, a mean relative error within 1.4%, and the coefficient of determination higher than 0.9. Furthermore, the proposed technique may easily be used for other electrical devices where PWM is employed.

Keywords: photovoltaic systems, pulse width modulation, monitoring, Labview

Abbreviations

| | |
|---|---|
| BCC | Battery charge controller |
| DAS | Data acquisition system |
| DC | Direct current |
| $d_f$ | Duty factor of battery or PV array |
| FIFO | Fist-In First-Out |
| $G_I$ (W/m$^2$) | Total irradiance in plane of the array |
| GUI | Graphical user interface |
| $I_A$(A) | Array current |
| $i_{A,average}$ | Average current of the PV array |
| $i_{A,p}$ | 'High' state of current of PV array |
| $i_{A,rsm}$ | True root mean square current of the PV array. |
| $I_L$ (A) | Load current |

ACCEPTED MANUSCRIPT

| | |
|---|---|
| $I_S$ (A) | Battery current |
| LED | Light emitting diode |
| IEC | International Electrotechnical Commission |
| MAPE | Mean absolute percentage error |
| MPPT | Maximum power point tracker |
| MRE | Mean relative error |
| PE | Percent error |
| PWM | Pulse width modulation |
| $R^2$ | Determination coefficient |
| SAPV | Stand-alone photovoltaic |
| SHSs | Solar home systems |
| SOC | State-of-charge |
| $T_m$ (ºC) | Module temperature |
| $V_A$ (V) | Array output voltage |
| $v_{A,average}$ | Average voltage of the PV array |
| $v_{A,rsm}$ | True root mean square voltage of the PV array |
| $v_{A,S}$ | Voltage when the array and battery are connected |
| $v_{A,OC}$ | Open-circuit voltage at weather conditions |
| $V_L$ (V) | Load voltage |
| $V_S$ (V) | Battery voltage |

## 1. Introduction

Energy objectives for "Horizon 2020" stress to increase the share of renewable energy to 20% in the energy mix and to improve the energy efficiency [1]. Thus, access to modern energy services is essential for economic development and human wellbeing [2–4]. In this sense, solar systems can provide electricity in areas and promote development across all sectors, from health to education. These types of systems are being used in several applications where there is enough solar energy to meet the electricity needs [5–7]. Solar power together with wind power represented 90% of 2015 investments in renewable power due to, amongst other things, the cost reduction of solar photovoltaic (PV) modules by 80 % and wind turbines by a third [8]. Furthermore, wind and solar power will continue to be the main technologies for renewable energy investment until 2020, with approximately 140 billion investment each per year [9].

It must be highlighted that photovoltaic systems can play an important role in rural electrification. More than one billion people in the world live without access to electricity. The majority of them live far from national electricity grids in rural areas [10], where the cost of delivering electricity requires huge investments to establish transmission and distribution grids [11]. Stand-alone photovoltaic systems have been considered a good alternative for places that are far from a conventional power generation system [12]. Solar home systems (SHSs), a type of SAPV system, have grown in many developing countries, with installations now surpassing more than six million [10]. Africa, Asia and America have by far the largest off-grid potential, making the market of SAPV systems on these continents very interesting [13]. Moreover, it has been observed in developed countries that the interest of public for "leaving the grid" or "living off-grid" is lower owing to continuous reduction in PV prices and a similar trend for battery storage [14].

An SAPV system consists of a PV generator connected to a battery charge controller (BCC), a battery system, and a stand-alone inverter if there are AC loads, Figure 1. A BCC is an essential element of an SAPV, as it regulates the flow of electricity from the PV generator to the battery, and from the battery to the load. It can regulate the current and voltage of the PV generator in order to prevent battery over-

ACCEPTED MANUSCRIPT

discharging and overcharging. BCCs can be ranked by the method used to regulate the current from the solar modules to the batteries. Pulse Width Modulation (PWM) and the Maximum Power Point Tracker (MPPT) techniques are the most widely used.

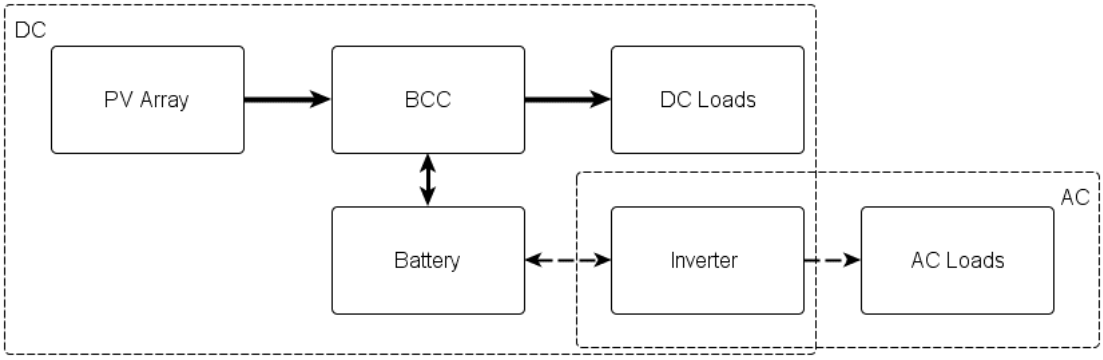


*Figure 1 Simplified block diagram of an SAPV*

For the long-term success of SAPV systems it is essential to secure the correct functioning of the systems, as well as to guarantee complete satisfaction and confidence to the users. To achieve these goals, it is necessary to manage a proper monitoring through DASs in order to achieve daily, monthly or annually derived parameters. Derived parameters, which are obtained during the operation, provide valuable information, not only to verify whether the design goals have been met, but also to improve the design and operation of SAPV systems and to assess the potential of this technology. DASs are employed to measure and collect operational data of PV systems to evaluate their performance under real conditions [15–17]. Therefore, the data obtained during the operation of photovoltaic systems are of great interest in determining the system performance [18], which will help not only to detect malfunctions but to optimize the system as well. Yasin Kabalci et al. detected an over sizing of a PV system by more than 40% [19] from measurements that were taken for a period of a year in real operating conditions.

One of the main goals of monitoring is to detect when an SAPV system shows sign of malfunction. An analysis of the rural electrification projects detected in Laos showed that 65% of the SHSs were not operative [20]. After five years of operation, another study found 45 percent of SHSs were out of order in Zacapa project in Guatemala. [21]. There have been many contributing factors but lack of maintenance after the installation may have played a leading role. In this sense, the way to ensure that systems operate as required is to monitor the system in the field [22], with the sensors, data acquisition devices, signals to be sensed, and monitoring techniques being the main issues to be taken into account [23]. The performance of PV systems can be obtained by monitored data which are processed to determine energy balances and energy efficiencies [24]. In such a way, the International Electrotechnical Commission (IEC) technical committee have drawn up the International Standard IIEC Standard 61724-1 [25], which is a technical revision of IEC 61724 that was published in 1998.

However, as has been referenced in the literature, there is a gap regarding power measurements when PWM battery charge controllers are used. PWM battery charge controllers modulate the charging current according to the battery state-of-charge (SOC), adjusting the width of current pulses. Therefore, a PWM battery charge controller provides the battery with a pulsed current-voltage instead of invariant constant current-voltage. This type of charging technique has advantages over invariant techniques such as increasing the battery life cycle and reducing the battery-charge time [26]. However, the former implies a challenge when addressing the monitoring of the system parameters. Admittedly, the updated Standard 61724-1 and the previous version provide solutions that may not take into account the idiosyncrasy of stand-alone photovoltaic systems with PWM battery charge controllers and batteries as the storage element [18,24]. Very expensive DASs are needed to provide a proper monitoring for these kinds of systems, which in most situations, cannot be afforded.

## 2. Background & objectives

Photovoltaic PWM battery charge controllers can be classified into two categories: series and shunt. Although the PWM signal frequency is a fixed value for a given BCC, in both types of BCCs it can range

ACCEPTED MANUSCRIPT

from ten to some hundreds of Hertz. Anyway, voltage and current pulses provided by PWM battery charge controllers are not simple sine waves but asymmetric square complex waveforms with components or harmonics at many frequencies [18]. The monitoring systems with medium and basic accuracy that are required for electrical output in PV applications should have a one minute maximum sampling interval. Sampling interval is defined as the time between samples [25]. According to this requirement, an instantaneous measurement of a PWM waveform may get a high, a low, or a transition value, Figure 2 (a). In this sense, a misleading measurement will be obtained if the monitoring process is not well designed and the particularities of this type of systems are not taken into account. Therefore, special measurement techniques or equipment may be required to provide a proper monitoring in SAPV systems with PWM controllers [27].

Another issue to consider is the calculated parameters from the measured ones (e.g. power). Power parameters can be calculated from voltage and current measurements. However, special attention should be paid when calculating parameters from simultaneously sampled variables, as DAS should be able to obtain simultaneous samples of current and voltage, or in a different sense, misleading measurements may result due the particularities of PWM signal and logging routines for measuring them [22,24]. For example, if the reading speed of the Data Logger is 60 channel/s and it cannot take synchronized measurements, there will be a delay between voltage and current measurements, Figure 2 (b). Moreover, the proper order of the operation should also be taken into account; otherwise, the calculated parameters could be inadequate. Hence, unless the DAS can synchronize measurements and the sampling frequency in compliance with the Annex A of the IEC 61724-1, it must be verified whether the product of the current and voltage is not calculated from voltage and current that are averaged. In fact, the product of averages is different from the average of products [28].

ACCEPTED MANUSCRIPT

ACCEPTED MANUSCRIPT

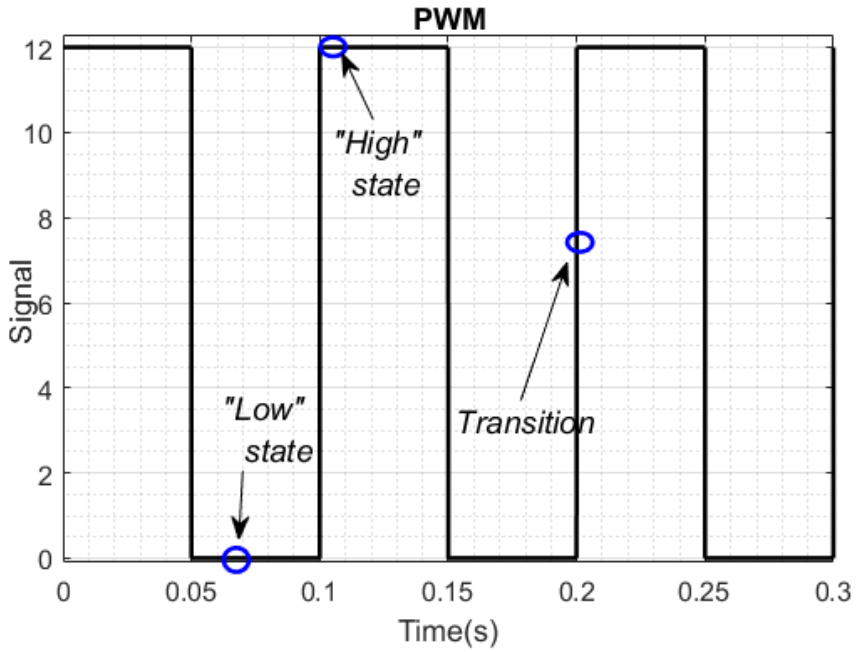


**(a)**

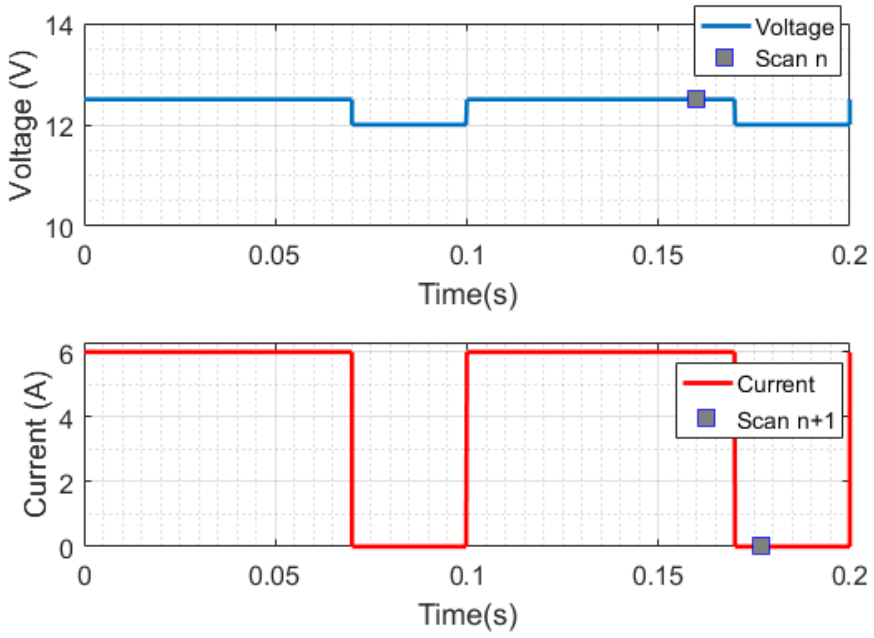


**(b)**

*Figure 2 (a) PWM waveform in SAPV systems. (b) Delay between channels when calculating parameters such as power from measured ones.*

At this point, it is clear that it is necessary to obtain the PWM signals to achieve a proper monitoring. In order to get a true PWM waveform, factors as the time response of the measurement sensors or transducers and the main frequency of the waveform help to select the most effective sampling interval. Selecting the wrong sampling interval may result in aliasing error and a loss of information. According to

ACCEPTED MANUSCRIPT

IEC Standard 61724-1, the sampling frequency should be increased up to 200 maximum frequency of the signal to achieve an accuracy of 1% in the reconstructed signal [25].

It should be stated that a high sampling frequency is possible to achieve if advanced equipment is used. The high reading speed which is needed to reconstruct this type of signal, the large amount of data collected and the issue of delay between channels can be solved with expensive DAS equipment, although this solution may be disproportionate considering the relative low cost[19] of the systems to be monitored. However, the above mentioned challenges can be faced if there is a shift of focus.

In the literature, an alternative method can be found which may improve the performance analysis of SAPV systems with photovoltaic BCCs with PWM and batteries as the storage element [24]. It is based on a translation of the energy parameters given by the Joint Research Centre and the IEC Standard 61724 into a new charge related parameter which is only based on the monitoring of currents [29]. In this sense, this method provides easy monitoring procedures to sample only average current parameters in SAPV systems with PWM battery charge controllers [18], where a complex monitoring system, sophisticated power estimation methods and simultaneous sampling at high sampling frequency are avoided. The sampling interval for the array current in SAPV systems with PWM battery charge controllers is one minute. The use of DC Hall effect transducers is recommended instead of a shunt resistor for measuring the array and battery currents.

However, and for the previously stated reasons, this method cannot calculate power parameters when required. Moreover, it cannot achieve the PWM waveform, which provides important information that may improve the performance analysis of the SAPV systems with storage, such as the PWM signal or duty factor; the term "duty cycle" is not used because with respect to 181™ IEEE Standard on Transitions, Pulses and Related Waveforms [23]. The duty factor can be used to calculate the losses related with battery high SOC. This type of capture losses, which are structural losses of SAPV systems, may mask other losses related to SAPV systems malfunctions. In this sense, the aim of this paper is to provide simple and effective new monitoring techniques for SAPV systems with PWM battery charge controllers that will manage to properly analyse SAPV systems performance, thus avoiding the use of expensive monitoring systems. Moreover, the techniques will provide not only the main features of the original PWM signals such as high and low states, but they will also manage to reconstruct them without using complex and expensive DASs. The paper will be focused on series PWM battery charge controllers, since they are the most widely used by the manufactures. Nevertheless, the proposed technique can easily be applied to the shunt PWM battery charge controllers. Moreover, the proposed technique has been validated by real field data that was measured by monitoring of an SAPV system with a series PWM controller. PWM signals are not only used in BCCs, but also for controlling electrical machines, for examples, induction motors are fed using various PWM techniques [30]. Moreover, one way to control the brightness of a light emitting diode (LED) is via PWM technique by adjusting the average LED current [31], thus obtaining specific benefits in terms of the degradation rate in comparison with direct current (DC). The frequency of the PWM dimming control signal is typically in the 100-400 Hz range [32]. In this way, the techniques here developed can be also applied to different applications where PWM signals are used. The manuscript has been organized as follows: the new monitoring techniques to be used in SAPV systems with PWM battery charge controllers and the mathematical background are shown in section 3. Thereafter, section 4 describes the application developed in LabVIEW® to validate the techniques previously described. In section 5, the results and analysis of the estimation of 'low' state, 'high' state and the $d_f$ of PWM waveforms are presented. Finally, the most relevant conclusions are given in Section 6.

## 3. Monitoring techniques for SAPV systems with PWM Battery charge controller

The duty factor measurement in PWM signals of SAPV systems can be obtained using different ways. Nathaniel et al.[22] proposed two techniques: the first one is based on the minimum, maximum and average PV voltages over a given recording interval, recording interval is defined as the time between records [25], and assumes that the square wave pulse is roughly constant over the recording interval. Recording interval should be divisible by the sampling frequency, which in turn depends on the signal frequency. In their study, 750ms of sampling interval and 1 min of recording interval were selected, that is 0.75 samples/s, and the frequency signal under study was 9.245Hz. The second one uses a counter to measure the $d_f$, where it is assigned a value of one to the $d_f$ if the measurement of the voltage waveform is

ACCEPTED MANUSCRIPT

higher than a reference voltage, and zero if it is lower. The average among ones and zeros over the recording interval estimates the average $d_f$ [22]. Both techniques are only to be applied to shunt PWM battery charge controllers. Moreover, the energy measurement error depends largely on the SOC of the battery, loads and irradiance, where a high value of energy measurement error was observed. Another possible solution is to use a microcontroller with a specific input pin and software. In the literature, there can be found different solutions to measure a waveform $d_f$ by using microcontrollers [33,34]. These techniques do not manage to reconstruct the PWM waveform and the sampling interval depends on the PWM frequency.

The method proposed in this paper does not depend on the signal frequency to select an appropriate sampling frequency for the battery charge controllers that are on the market. Furthermore, sampling interval can be one minute. As explained in the next section, the $d_f$ and the low state and high state of the PWM waveform can be estimated by sensing only average and true root mean square values of the measured PWM signal. Moreover, PWM waveforms can be reconstructed if the frequency is known or measured. As previously mentioned, the signal frequency of a PWM is a fixed value. In order to illustrate the technique here shown, the technique will be applied to both current and voltage PWM signals in the PV array. Moreover, the PV array current signal will be used to estimate the $d_f$. Therefore, 'ON time' will be considered as the time interval the PV array current waveform is in the high state. On the other hand, 'OFF time' will be the time interval when the PV array current waveform is in the low state.

Figure 3(a) shows the PWM array and battery voltages, meanwhile Figure 3 (b) shows the PWM array and battery current in a commercial series BCC. At has been previously mentioned, although the technique here shown will be illustrated considering a series PWM battery charge controller, the technique can be easily extrapolated to shunt ones. The frequency of a PWM signal for the BCC is 300 Hz (a 3.3ms period). As can be seen in these figures, the high state of PV array voltage waveforms corresponds with open circuit voltage which is reached by the array when the series BCC is open. Consequently, there is no array current at that moment (low state of PV array current waveform). On the other hand, during the 'On' interval, a BCC makes a connection between PV array and battery; therefore, battery voltage and array voltage operate at the same voltage ($V_{AS}$).

ACCEPTED MANUSCRIPT

ACCEPTED MANUSCRIPT

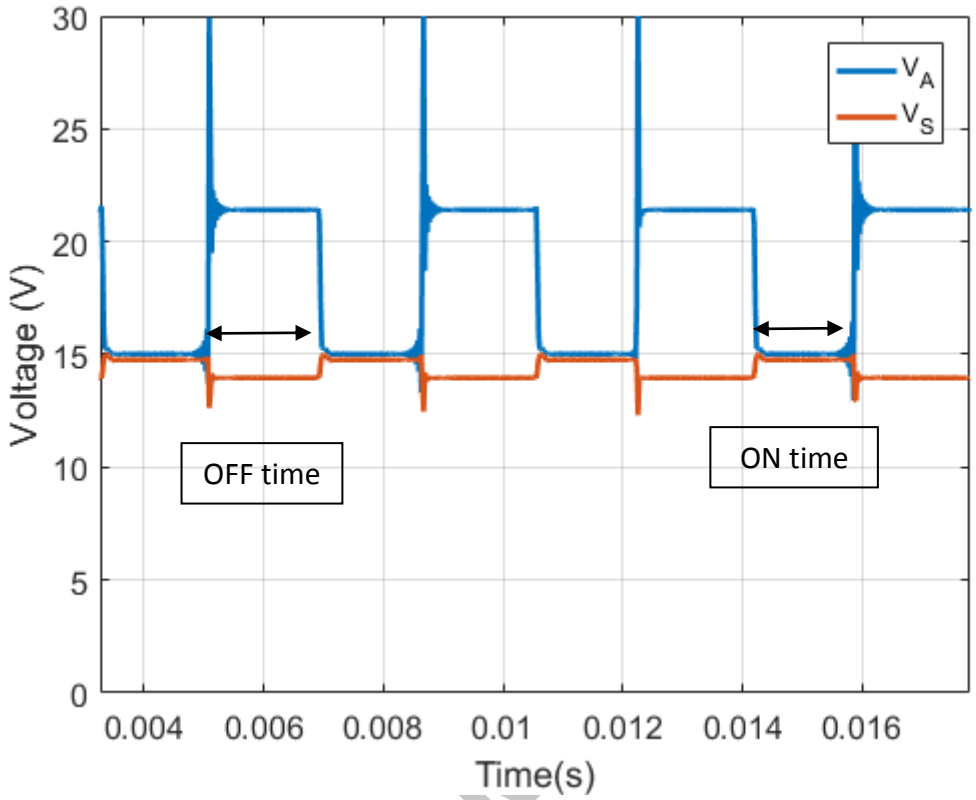


**a)**

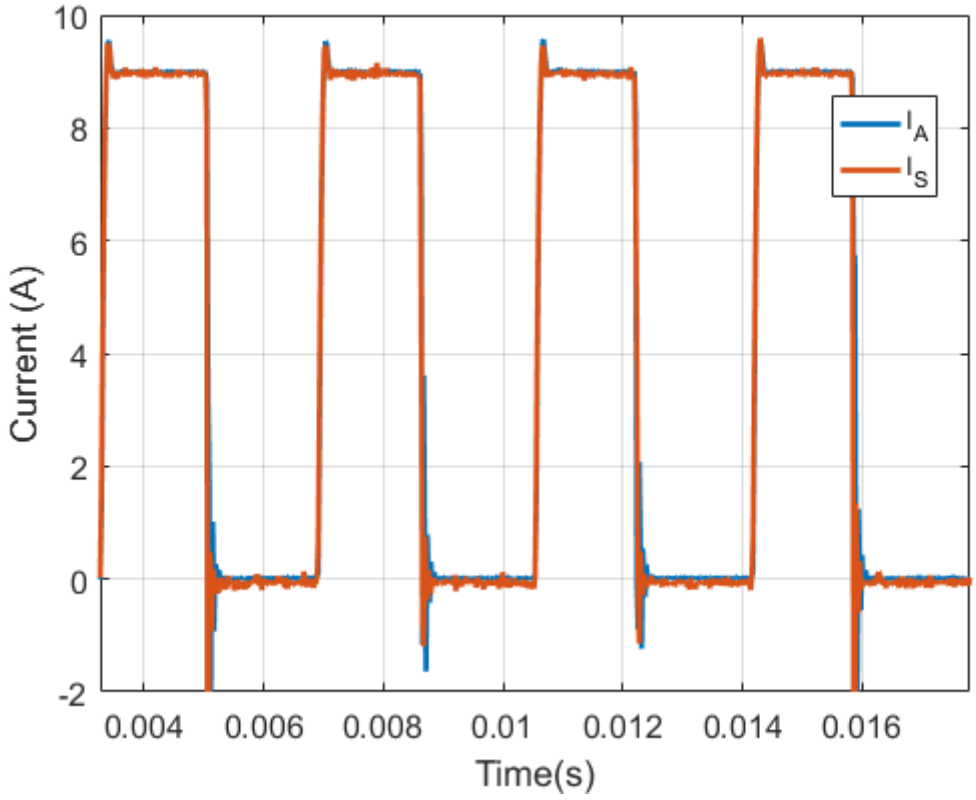


**b)**

*Figure 3(a) PV array and Battery Voltage. (b)* PV array and Battery Current without any load in a series PWM battery charge regulator.

ACCEPTED MANUSCRIPT

As will be shown later, the PWM current array waveforms can be defined if the $d_f$, frequency and the high state and low state of the PWM signal are known. The frequency is usually a fixed value in PWM battery charge controllers and it is assumed that the square wave pulse is approximately constant over the recording interval which will be one minute. Moreover, the proposed technique can be used when one state (low or high) of the signal is known; in the case study, the low state of the current will have a value of zero amps.

The $d_f$ and the high and low state parameters for the PWM waveform corresponding to the array current from other electrical parameters such as the average and the true root mean square array current are defined below. Both electrical parameters can easily be measured through current sensors and transducers.

The true root mean square and average PV array current can be expressed as follows, equations (1) and (2), respectively:

$$i_{A,rsm} = \sqrt{\frac{1}{T} \times \int_0^T i(t)^2 dt} \approx \sqrt{\frac{1}{T} \times \left( \int_0^{t_{ON}} {i_{A,p}}^2 dt + \int_{t_{ON}}^{t_{off}} 0^2 dt \right)} = \sqrt{\frac{1}{T} \times {i_{A,p}}^2 \times [t_{ON} - 0]} = i_{A,p} \times \sqrt{\frac{t_{ON}}{T}} = i_{A,p} \times \sqrt{d_f} \quad (1)$$

$$i_{A,average} = \frac{1}{T} \times \int_0^T i(t) dt \approx \frac{1}{T} \times \left( \int_0^{t_{ON}} i_{A,p}\, dt + \int_{t_{ON}}^{t_{off}} 0\, dt \right) = \frac{1}{T} \times i_{A,p} \times [t_{ON} - 0] = i_{A,p} \times \frac{t_{ON}}{T} = i_{A,p} \times d_f \quad (2)$$

Where $i_{A,rsm}$ depicts the true root mean square current of the PV array, $i_{A,average}$ represents the average current of a PV array, $i_{A,p}$ is the high state of PV array current and $d_f$ depicts the duty factor of PV array current.

Through equations (1) and (2) the signal duty factor can be obtained as:

$$d_f = \frac{{i_{A,average}}^2(A)}{{i_{A,rsm}}^2(A)} \quad (3)$$

Once $d_f$ is calculated, the 'high' state of PV array current can be expressed as:

$$i_{A,p} = \frac{i_{A,average(A)}}{d_f} = \frac{{i_{A,rsm}}^2(A)}{i_{A,average(A)}} \quad (4)$$

When the most important PWM current parameters that may define the PWM array waveform ($d_f$ and high state current of PV array) are achieved, they may be used to reconstruct the signal. In this way, PV array current can be defined as follows:

$$I_A(t) = \begin{cases} i_{A,p} & \text{PWM ON} \\ 0 & \text{PWM OFF} \end{cases} \quad (5)$$

Likewise, the PWM array voltage waveform will be obtained, and together with the PWM PV array current waveform can be used to calculate the array power of SAPV systems. The solution proposed in this paper, is to measure the average PV array voltage and true root mean square PV array voltage. The following equations allow an estimation of $v_{A,OC}$ and $v_{A,S}$

$$v_{A,average} = \frac{1}{T} \times \int_0^T v(t) dt \approx \frac{1}{T} \times \left( \int_0^{t_{ON}} v_{A,s}\, dt + \int_{t_{ON}}^{t_{off}} v_{A,OC}\, dt \right) = \frac{1}{T} \times \left( v_{A,s} \times t_{ON} + v_{A,OC} \times [t_{OFF} - t_{ON}] \right) = v_{A,s} \times d_f + v_{A,OC} \times (1 - d_f) \quad (6)$$

$$v_{A,rsm} = \sqrt{\frac{1}{T} \times \int_0^T v(t)^2 dt} \approx \sqrt{\frac{1}{T} \times \left( \int_0^{t_{ON}} {v_{A,s}}^2 dt + \int_{t_{ON}}^{t_{off}} {v_{A,OC}}^2 dt \right)} = \sqrt{\frac{1}{T} \times \left( {v_{A,s}}^2 \times [t_{ON} - 0] + {v_{A,OC}}^2 \times [t_{OFF} - t_{ON}] \right)} = \sqrt{\left( {v_{A,s}}^2 \times d_f + {v_{A,OC}}^2 \times [(1 - d_f)] \right)} \quad (7)$$

where $v_{A,average}$ and $v_{A,rsm}$ are the average voltage of the PV array and the true root mean square voltage of the PV array, respectively. $v_{A,S}$ represents the voltage when the array and battery are connected, $v_{A,OC}$ is the open-circuit voltage at weather conditions. The $d_f$ is the same as obtained in Eq.(3).

ACCEPTED MANUSCRIPT

From Eq.(6) and Eq.(7) $v_{A,OC}$ and $v_{A,S}$ can be obtained:

$$v_{A,OC}{}^2 \times (1 - d_f) - v_{A,OC} \times 2 \times v_{A,average} \times (1 - d_f) - v_{A,rsm}{}^2 \times (d_f) + v_{A,average}{}^2 \quad (8)$$

$$v_{A,S} = \frac{v_{A,average} - v_{A,OC} \times (1 - d_f)}{d_f} \quad (9)$$

In this way, the PV array voltage can be defined as follows:

$$V_A(t) = \begin{cases} v_{A,S} & \text{PWM ON} \\ v_{A,OC} & \text{PWM OFF} \end{cases} \quad (10)$$

In summary, the proposed technique described above is based on the use of the basic electronic concept such as root mean square and average of a signal. The first step to be accomplished is to determine the $d_f$ of the PWM array current waveform. The second step is to estimate the high stated of the PWM current waveforms of the array and the third step is to establish the low and high state of the PWM voltage waveforms of the array.

4. Material and experimental procedure to validate the developed technique

An SAPV system with its corresponding sensors and data logger device have been installed in the Higher Polytechnic School of Jaén (latitude: 37 deg 47´00´´ N and longitude 3 deg 47´ 0´´ W) in order to provide the necessary data to validate the monitoring methodology mentioned before. The modules are tilted 50 degrees to the horizontal, facing south. The SAPV system consists of a power generator with two commercial photovoltaic modules connected in parallel, a series PWM battery charge controller (MorningStar ProStar-15), a 12V 200Ah lead-acid battery and a load box which manages to set different daily load profiles for the battery discharge. Additional information about the main characteristics of the PV generator can be found in Table 1.

**a)** **b)**

*Figure 4 Stand-alone Photovoltaic System (a) PV generator and (b) BCC, sensors and traducers.*

*Table 1* Main electrical Characteristics of SAPV system used to carry out this study

| **Main electrical characteristics** | | **Value** |
|---|---|---|
| PV array | Module number | 2 |
| | $I_{SC,STC,array}$ (A) | 12.14 |
| | $I_{MPP,STC,array}$ (A) | 11.46 |
| | $V_{OC,STC,array}$ (V) | 21.97 |
| | $V_{MPP,STC,array}$ (V) | 17.46 |
| | Module efficiency (%) | 12.88 |
| Battery | Capacity | 200 Ah @10hr-rate |
| | $V_S$ | 12V |

ACCEPTED MANUSCRIPT

| | |
|---|---|
| Battery Charge Controller | Series PWM BCC. MORNING STAR. ProStar-15 |

Various transducers and sensors measure the parameters indicated in Table 2. The parameters, such as array, load and battery voltage ($V_A$, $V_L$ and $V_S$), are measured directly by the DAS. Calibrated shunt resistances are used to measure the PV array current ($I_A$) and battery current ($I_S$) and load current ($I_L$). In addition, a PT100 (platinum resistor) is used to measure the module temperature through a four wire measurement. Following the instructions of Annex B given by the IEC Standard 61724-1, PT100 is located on the rear side of one module at the center of a cell close to the center of the module avoiding boundaries between cells[25]. In-plane irradiance is measured by means of a calibrated cell with the same technology of the photovoltaic modules considered. Table 3 shows the rated values of the main features of the transducers and sensors.

*Table 2* Measured and recorded parameters.

| **Measured and recorded parameters** | **Symbol (unit)** |
|---|---|
| Array current | $I_A$(A) |
| Battery current | $I_S$ (A) |
| Load Current | $I_L$ (A) |
| Array output voltage | $V_A$ (V) |
| Battery voltage | $V_S$ (V) |
| Load voltage | $V_L$ (V) |
| Module temperature | $T_m$ (ºC) |
| Total irradiance in plane of the array | $G_I$ (W/m$^2$) |

*Table 3* Main features of the transducers and sensors.

| **Transducers and sensor** | **Features** |
|---|---|
| Shunt ($I_A$) | 25A-150mV |
| Shunt ($I_S$) | 25A-150mV |
| Shunt ($I_L$) | 25A-150mV |
| PT100 | In accordance with IEC 60751 W0.15 (Class A) -100°C to +450°C |

The SAPV system monitored and the data collected are used to compare the proposed technique with the one given by Annex A of the IEC 61724-1 Standard, where the sampling frequency is set at 200 times the maximum frequency of the signal [25]. Measured parameters are collected by high accuracy DAS, that measure the PV array, battery and load current and voltage. On the other hand, the sampling frequency for the techniques presented in this paper for the current and voltage and module temperature and irradiance is one sample per minute. The hardware used to collect the data is cDAQ-9172 chassis and NI 9229, NI 9217 and NI9205 modules. The NI cDAQ-9172 is an eight-slot USB chassis. It is used to measure the considered parameters and to control the loads. In addition, Table 4 shows the main features of the modules that are used for the monitoring process.

*Table 4* Main features of the modules use for measuring[35].

| **Module** | **Parameter** | **Features** | | |
|---|---|---|---|---|
| | | **Type of ADC** | **Number of bits** | **Sampling frequency during the test** |
| NI 9217 | $T_m$ | Delta-sigma | 24 Bit | 100 S/s |
| NI 9229 | $V_A$<br>$V_S$<br>$V_L$ | Delta-Sigma (with analog prefiltering) | 24 Bit | 60 kS/s |
| NI9205 | $I_A$ (Shunt resistor)<br>$I_S$ (Shunt resistor)<br>$I_L$ (Shunt resistor)<br>$G_I$ (Calibrated cell) | Delta-sigma | 16 Bit | 250 kS/s |

ACCEPTED MANUSCRIPT

The measurements are performed by cDAQ-9172 chassis and NI 9229, NI 9217 and NI9205 high quality modules. A source of uncertainty associated with these devices is the Absolute Accuracy (AA). The absolute accuracy is defined as the worst-case of a measurement for a given DAQ device at a specified range where it is taken into account the temperature variations, worst case component tolerances of the devices, thermal hysteresis…[36]

The AA of NI 9229 can be calculated throughout the entire operating temperature range (-40 to 70 ºC) as:

$$AA_{NI\ 9229} = \pm[(InputReading\ \times GainError) + (Range\ \times OffsetError) + InputNoise] \quad (11)$$

Where Input Reading is the value which is being measured, Gain error corresponds to the percentage accuracy based on the input gain, Range is the span which has been configured for the device, OffsetError is the maximum offset error and InputNoise is the error the device introduces to a measurement by the device itself.

*Table 5* NI 9229 Accuracy [37] *:*

| **Measurement Conditions** | **Percent of Reading** (Gain Error) | **Percent of Range** (Offset Error) (range equals 62.64V) |
|---|---|---|
| Typical (25ºC, ± 5ºC) | ±0.03% | ±0.008% |
| Maximum (-40ºC to 70ºC) | ±0.13% | ±0.05% |

The calculation of the $AA_{NI\ 9229}$ can be estimated with errors parameters of the previous table and an input value of 320 μVrms, according to the manufacturer. DAQ has been operating in the laboratory with controlled temperature (25 ± 5ºC), therefore, $AA_{NI\ 9229}$ could be:

$$AA_{NI\ 9229} = \pm[(InputReading\ \times 0.00003) + (62.61\,V\ \times 0.00008) + 320\mu V] = \pm[(InputReading\ \times 0.00003) + (5.0088mV) + 320\mu V] = \pm[(InputReading\ \times 0.00003) + 5.3288mV\ ] \quad (12)$$

Where $AA_{NI9229}$ is the uncertainty due to absolute accuracy of the measurement of $V_A$, $V_S$ and $V_L$.

Similarly, the AA of NI 9205 can be calculated as [38]:

$$AA_{NI\ 9205} = \pm[(InputReading\ \times GainError) + (Range\ \times OffsetError) + Noise\ Uncertainty] \quad (13)$$

Where

$$GainError = Residual\ Gain\ Error + Gain\ Tempco \times Temp\ Change\ from\ Last\ Internal\ Cal + Reference\ Tempco \times Temp\ Change\ from\ Last\ External\ Cal \quad (14)$$

$$Offset\ Error = Residual\ Offset\ Error\ +\ Offset\ Tempco\ \times\ Temp\ Change\ from\ Last\ Internal\ Cal + INL\ Error \quad (15)$$

$$Noise\ Uncertainty = \frac{(Random\ Noise \times 3)}{\sqrt{100}}\ for\ a\ coverage\ factor\ of\ 3\ \sigma\ and\ averaging\ 100\ points \quad (16)$$

In this case, the following assumptions are needed to determine the $AA_{NI\ 9205}$ at full scale on the analog input channels:

- Temperature Change from Last External Cal=70ºC
- Temperature Change from Last Internal Cal=1ºC
- Number of Reading=100
- Coverage Factor = 3 σ.

Input Noise error will depend on filter settings and the noise are assumed that is a Gaussian distribution with yields 99.73% confidence [36]

ACCEPTED MANUSCRIPT

*Table 6* NI 9205 Accuracy [38]

| Range | Residual gain error | Residual offset error | Offset tempco | Gain tempco | Reference tempco | INL error | Random Noise, σ |
|---|---|---|---|---|---|---|---|
| ± 10 V Range | 115 ppm of reading | 20 ppm of range | 44 ppm of range/°C | 11 ppm/°C | 5 | 76 ppm of range | 240 µV RMS |
| ± 5 V Range | 135 ppm of reading | 20 ppm of range | 47 ppm of range/°C | | | | 116 µV RMS |
| ± 1 V Range | 155 ppm of reading | 25 ppm of range | 66 ppm of range/°C | | | | 26 µV RMS |
| ± 0.1 V Range | 215 ppm of reading | 40 ppm of range | 162 ppm of range/°C | | | | 10 µV RMS |

The $AA_{NI\ 9205}$ at full scale with ± 1 V of the span is:

$$GainError = 155ppm + 11\frac{ppm}{ºC} \times 1ºC + 5\frac{ppm}{ºC} \times 70ºC = 516\,ppm$$

$$Offset\ Error = 25ppm + 66\frac{ppm}{ºC} \times 1ºC + 76ppm = 167ppm$$

$$Noise\ Uncertainty = \frac{(26\mu V \times 3)}{\sqrt{100}} = 7.8uV$$

$AA_{NI\ 9205} = \pm[(InputReading \times 516\,ppm) + (1V \times 167ppm) + 10uV] = \pm[(InputReading \times 516\,ppm) + (1V \times 167ppm) + 7.8uV] = \pm[(InputReading \times 0.00000516) + (1V \times 0.00000167) + 10uV] = \pm[(InputReading \times 0.000516) + (1V \times 0.000167) + 7.8uV] = \pm[(InputReading \times 0.000516) + 174.8uV]$
(17)

Where $AA_{NI\ 9205}$ is the uncertainty due to absolute accuracy of a measurement of $I_A$, $I_S$, $I_L$ and $G_L$

On the other hand, the temperature accuracy of NI 9217 using 4 wire mode is [39]:

*Table 7* NI 9217 Accuracy [39]*:*

| Measured Value | Typical (25 °C) | Maximum (-40 to 70 °C) |
|---|---|---|
| -200 °C to 150 °C | 0.15 °C | 0.35 °C |
| 150 °C to 850 °C | 0.20 °C | 1.0 °C |

$$TA_{NI\ 9217} = \pm 0.15\ ℃$$

Where $TA_{NI\ 9217}$ is the uncertainty due to temperature accuracy of a measurement of $T_m$.

As mentioned above, $V_A$, $V_L$ and $V_S$ are measured directly by the DAS, thus the source of uncertainty is $AA_{NI\ 9229}$. There is no specific knowledge about the absolute accuracy distribution. In this sense, a rectangular distribution is assumed for the estimation of standard uncertainty and it is estimated as:

$$u_v = \sqrt{\left(\frac{AA_{NI\ 9229}}{\sqrt{3}}\right)^2} = \sqrt{\left(\frac{(InputReading \times 0.00003) + 5.3288mV}{\sqrt{3}}\right)^2} \quad (18)$$

In case of the current measurement, there is also another source of uncertainty associated to the calibrated shunt resistor. Accuracy class of the shunt resistor is 0.5, thus, accuracy is ±0.5%. There is also a lack information about the accuracy distribution, so a rectangular distribution is also assumed. The standard uncertainty of the component is:

$$u_{Shut} = \sqrt{\left(\frac{InputReading \times Accuracy}{\sqrt{3}}\right)^2} = \sqrt{\left(\frac{InputReading \times 0.005}{\sqrt{3}}\right)^2} \quad (19)$$

The standard uncertainty of the shunt and the standard uncertainty of the module used to measure the voltage drop across the shunt resistor are independent. Hence, the resulting combined uncertainty ($u_i$) of $I_A$, $I_S$ and $I_L$ is estimated as:

ACCEPTED MANUSCRIPT

$$u_i = \sqrt{\left(\frac{AA_{NI\ 9205}}{\sqrt{3}}\right)^2 + u_{Shut}} == \sqrt{\left(\frac{(InputReading \times 0.000516)+174.8uV}{\sqrt{3}}\right)^2 + \left(\frac{InputReading \times 0.005}{\sqrt{3}}\right)^2} \quad (20)$$

There are three sources of uncertainty associated to a temperature measurement. The first one is the absolute accuracy of the DAQ. The second one is introduced by the sensor. In this case, PT100 has been used which is Class A, thus, the value of the tolerance is ±0.35ºC and the standard uncertainty is:

$$u_{PT\ 100} = \sqrt{\left(\frac{0.35}{\sqrt{3}}\right)^2} \quad (21)$$

The third source of temperature uncertainty is because there is a drop in temperature between cell and backskin. The module temperature should be adjusted +3º with a total range of ±1ºC to estimate cell temperature [36] and the uncertainty is calculated as:

$$u_{Tc} = \sqrt{\left(\frac{1}{\sqrt{3}}\right)^2} \quad (22)$$

The combined uncertainty of temperature is estimated as the root sum of squares of the associated uncertainties:

$$u_T = \sqrt{\left(\frac{A_{NI\ 9217}}{\sqrt{3}}\right)^2 + u_{PT\ 100} + u_{Tc}} = \sqrt{\left(\frac{0.15}{\sqrt{3}}\right)^2 + \left(\frac{0.35}{\sqrt{3}}\right)^2 + \left(\frac{1}{\sqrt{3}}\right)^2} = 0.81ºC \quad (23)$$

Table 8 provides the absolute accuracy of the devices and the standard uncertainties of the measurement. This analysis is based on the recommendations and requirements of the guide JCGM 100:2008[40].

*Table 8* Absolute accuracy and standard deviation of the devices and components.

| **Device** | **Absolute accuracy / Standard uncertainties** |
|---|---|
| NI 9229 | $AA_{NI\ 9229} = \pm[(InputReading\ \times 0.00003) + 5.3288mV\ ]$ |
| NI 9229 | $AA_{NI\ 9205} = \pm[(InputReading\ \times 0.000516) + 174.8uV]$ |
| NI 9217 | $TA_{NI\ 9217} = \pm 0.15$ °C |
| $u_V$ ($V_A$,$V_L$ and $V_S$) | $u_v = \sqrt{\left(\frac{(InputReading\ \times 0.00003) + 5.3288mV}{\sqrt{3}}\right)^2}$ |
| $u_i$ ($I_A$,$I_L$ and $I_S$) | $u_i = \sqrt{\left(\frac{(InputReading\ \times 0.000516) + 174.8uV}{\sqrt{3}}\right)^2 + \left(\frac{InputReading\ \times 0.005}{\sqrt{3}}\right)^2}$ |
| $u_T$ | $u_T = 0.81ºC$ |

The monitoring system has been controlled by a proper interface that was developed in LabVIEW ®. LabVIEW provides an easy and powerful graphical interface for instrument management [41] where users are able to develop a sophisticated application without advanced knowledge of DAS design and with no need for developing complex data processing algorithms. The tasks of the application are focused on managing the communication with DAS to determine when the measurement of different parameters should be acquired and to control the load profile. Moreover, measured parameters are processed, stored and displayed.

The block diagram of the application is illustrated in Figure 5. The application has been divided into an initialization step in order to configure the channels and the timing and three different subroutines that can work in parallel. The first one is related to the acquisition data, the second one is focused on the load control and the last one manages to display and store the measured data. For the initialization steps and first subroutine, DAQmx drivers have been used to develop the channel setting, timing settings and the data acquisition process. Although the first and third subroutines can work in parallel, they are managed with producer/consumer architecture, where the first subroutine is the producer and the third is the consumer; therefore, the third subroutine is waiting for the measured parameters that the first subroutine

ACCEPTED MANUSCRIPT

has measured. Producer/consumer architecture was selected because the first and the third process can run simultaneously and continuously and they can run at different speeds[42]. Communication between producer and consumer loops is done by using data queues; it works according to first-in/first-out (FIFO). In this way, the loss of data can be avoided.

A graphical user interface (GUI) was developed in order to display the measured parameters (currents, voltages, irradiance and module temperature); Figure 6 (a). Measured parameters are updated each minute when the data are collected in the graphs. Buttons, tabs, switches and a list of properties have been used to provide an easy way to configure the parameters that are required by DAQmx used, Figure 6 (b, c).

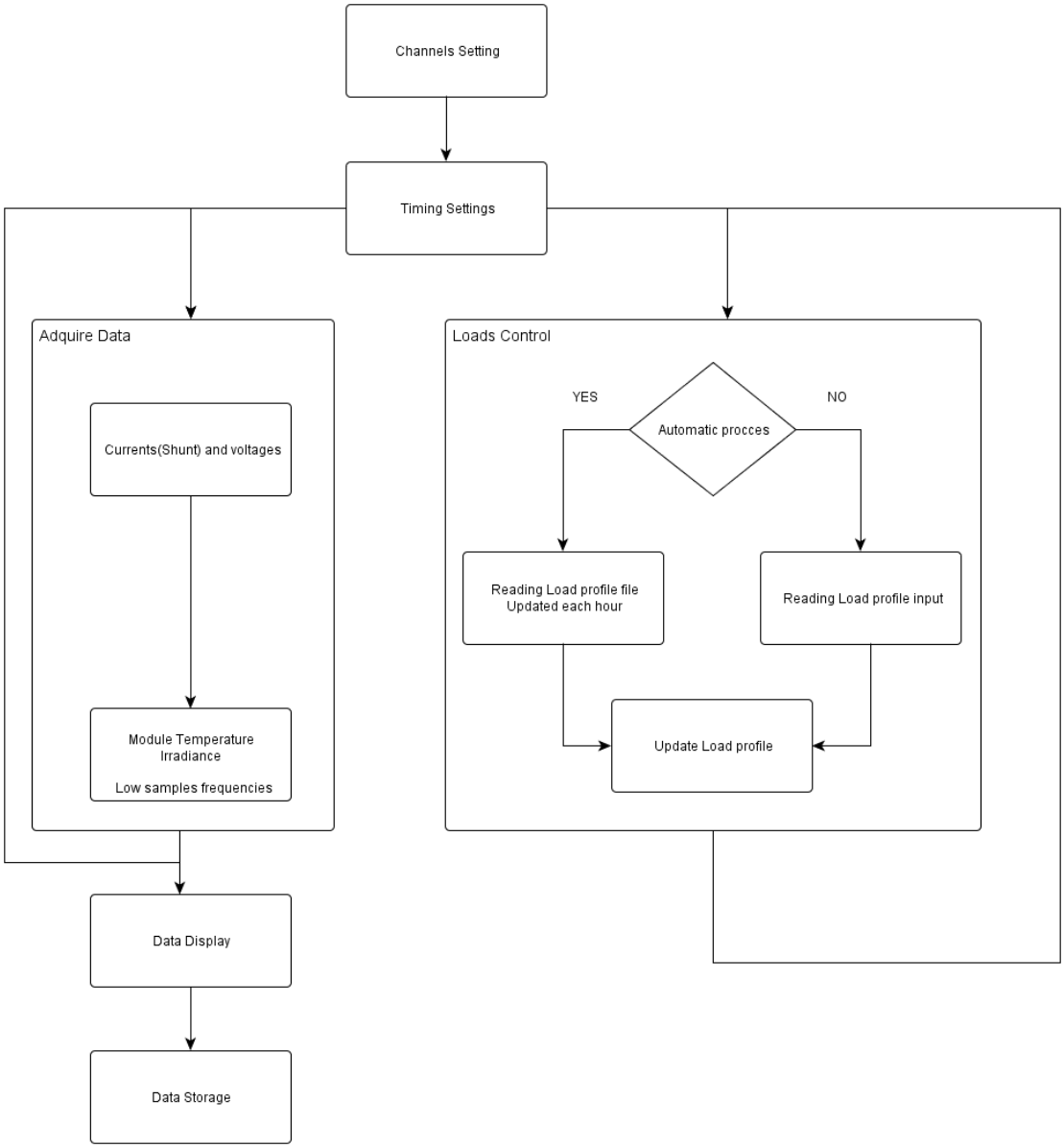


*Figure 5* Block diagram of developed program to monitor SAPV system.

ACCEPTED MANUSCRIPT

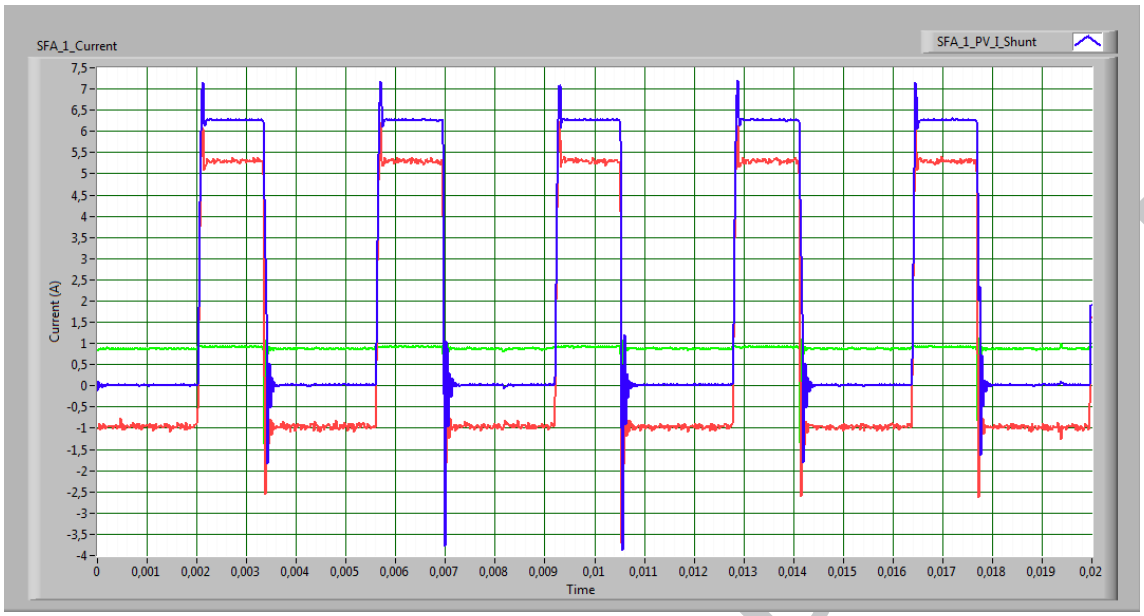


**a)**

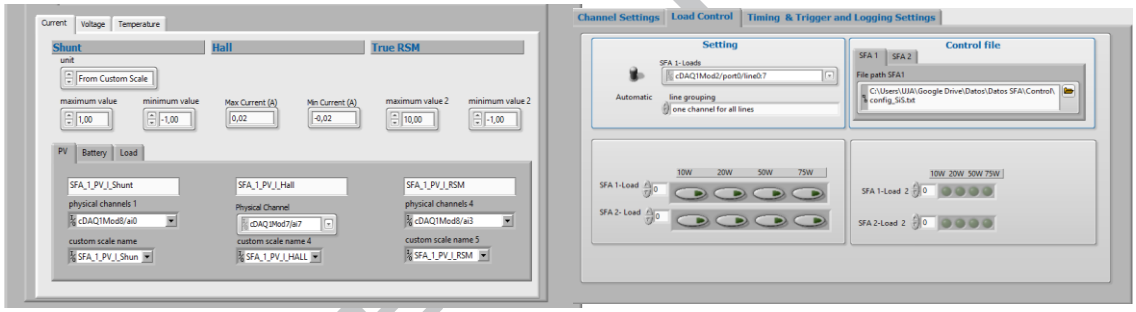


**b)** **c)**

*Figure 6 (a)* Graphical user interface for SAPV system monitoring. (b, c) Buttons, tabs, list of properties and switches to configure the measurement properties.

## 5. Results and discussions

Measured parameters are sampled at the corresponding sampling frequency recommended by the IEC 61724-1 Standard. Current parameters are measured with a shunt resistor and voltages are measured directly by DAS. In this sense, the original PWM waveform is achieved. In order to validate the technique mentioned before, these data are processed by software to calculate mean current, mean voltage, true root mean square current and voltage of the measured parameters in full compliance with 181™ IEEE Standard on Transitions, Pulses and Related Waveforms [23]. These estimated parameters will be used in order to reconstruct the PWM signals. A computerized tool, developed by Matlab (MATrix LABoratory), has been designed to process the collected data. Moreover, the error made in the estimation of significant PWM waveform parameters between measured and reconstructed waveforms has been calculated. In this sense, statistical criteria have been used to evaluate the estimation of parameters such as $d_f$, the high state of PV array current, and the high state and low state of the array voltage. The reference values are the parameters that are measured at a high sampling frequency with full compliance with the Annex A of the IEC 61724-1, as indicated above. The performance of the estimated parameters was assessed based on: percentage error (PE), Eq.(24) mean absolute percentage error (MAPE), Eq.(25), the mean relative error (MRE), Eq.(26) and the determination coefficient (R), Eq.(27).

$$\mathrm{PE}\ (\%) = 100 \times \frac{(X_{filtered} - X_{ref})}{X_{ref}} \tag{24}$$

ACCEPTED MANUSCRIPT

$$\text{MAPE}(\%) = \frac{100}{N} \times \sum_{i=1}^{N} \left| \frac{(X_{filtered} - X_{ref})}{X_{ref}} \right| \quad (25)$$

$$\text{MRE}(\%) = \frac{100}{N} \times \sum_{i=1}^{N} \frac{(X_{filtered} - X_{ref})}{X_{ref}} \quad (26)$$

$$R\ (\%) = \frac{\sum_{i=1}^{N}(X_{ref} - \bar{X}_{ref}) \times \sum_{i=1}^{N}(X_{filtered} - \bar{X}_{filtered})}{\sqrt{\sum_{i=1}^{N}(X_{ref} - \bar{X}_{ref})^2 \times \sum_{i=1}^{N}(X_{filtered} - \bar{X}_{filtered})^2}} \quad (27)$$

where N represents the number of samples and X is the parameter considered. The samples collected at the high frequency have been taken as the reference values.

Figure 7 shows the correlation between the duty factor that has been estimated using equation 3 and the algorithm that is described in 181™ IEEE Standard on Transitions, Pulses and Related Waveforms [23]. As can be observed, the PE is practically marginal for duty factors that are above 0.2. The PE becomes higher but always below 10% when the BCC with PWM provides a very low duty factor, i.e. when a high battery SOC is reached. Due to a high SOC, the energy that goes to the battery from the PV array may be negligible; therefore, the energy error for these small duty factors will be considerably diminished. The duty factor parameter, apart from being needed to reconstruct the PWM signal, constitutes an important parameter to calculate the energy that is being wasted in this battery charge step [22].

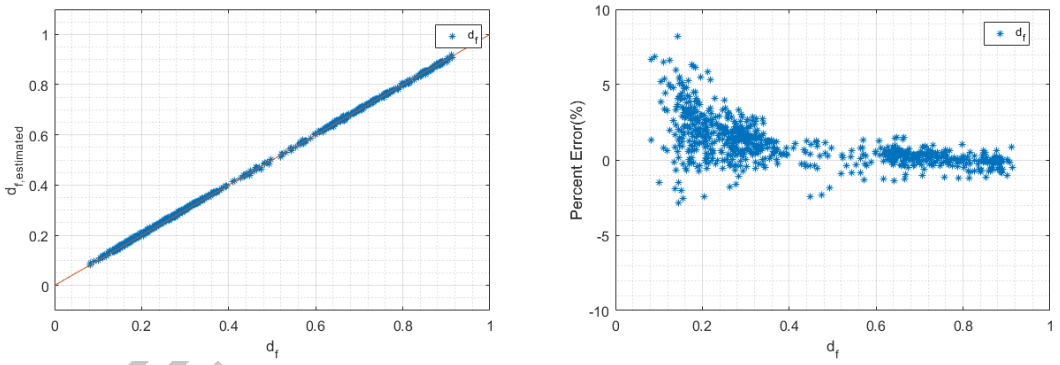


*Figure 7 Measuring $d_f$ at high sampling frequency and estimated.*

Figure 8, Figure 9 and Figure 10 respectively show the correlation between the measured versus estimated electrical parameters $I_{AP}$, $V_{A,S}$ and $V_{A,OC}$ that are collected at a high sampling frequency and the proposed technique. As can be seen, the PE calculated is lower than 5% for the estimated parameters. It should be highlighted that the errors, when estimating the $d_f$, $I_{AP}$ and $V_{AS}$, increase when the $d_f$ decreases as shown in Figure 8 and Figure 9. On the contrary, the PE of $V_{OC}$ increases when the $d_f$ is close to one. $V_{OC}$ is the voltage when the PV array and the battery are not connected (PWM OFF and high state of the waveform). This state of the voltage waveform is proportional to the subtraction of one minus $d_f$. Thus, when the current signal receives a high state, the voltage signal is in the low state and vice versa. Therefore, $V_{OC}$ follows an opposite trend of $I_{AP}$ and $V_{AS}$. Figure 9 and Figure 10 show the appropriate voltage range in order to evaluate the error tendency.

ACCEPTED MANUSCRIPT

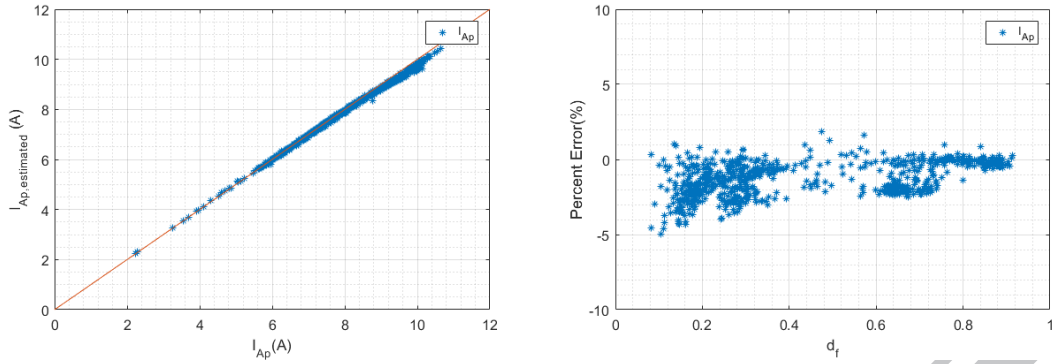


**a)** **b)**

*Figure 8 Measuring current at high sampling frequency and estimated.*

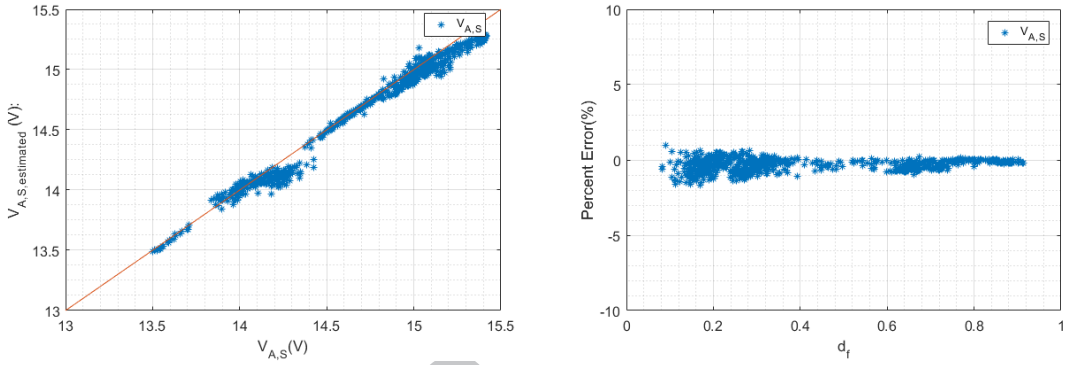


**a)** **b)**

*Figure 9 measuring array open circuit voltage at high sampling frequency and estimated.*

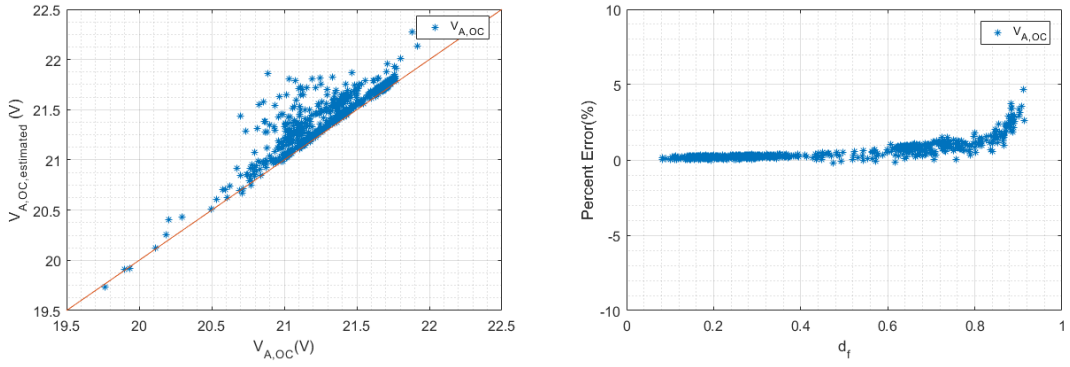


**a)** **b)**

*Figure 10 measuring battery voltage at high sampling frequency and estimated.*

Statistical error indicators including MAPE, MRE and $R^2$ are summarized in Table 9. The MAPE is within 1.4%, also the MRE is lower than 1.4% and $R^2$ is higher than 0.9 for estimated parameters under study. Thus, it can be concluded that the filters, such as TRMS transducers and average sensors, used to calculate electrical parameters of PWM waveform provide good agreement between the sampling frequency recommended by the IEC 61724-1 Standard and the proposed technique. A high sampling frequency of the measurement that involves high cost has been compared versus a technique that allows a sampling frequency of one minute which avoids not only a huge amount of collected data but the drawbacks derived from the delay between channels, and therefore, less expensive DAS.

ACCEPTED MANUSCRIPT

*Table 9 Mean absolute percentage error (MAPE), mean absolute error (MRE) and determination coefficient ($R^2$) between measured and estimated parameters under study using Eqs. (25), (26) and (27)*

| Parameter | MAPE(%) | MRE (%) | $R^2$ |
|---|---|---|---|
| $d_f$ | 1.28 | 1.06 | >0.99 |
| $I_{AP}$ | 1.38 | -1.32 | >0.99 |
| $V_{As}$ | 1.09 | -1.18 | >0.90 |
| $V_{AOC}$ | 0.66 | -0.56 | >0.90 |

As previously mentioned, once the low and high state and $d_f$ are estimated and the frequency is known or measured, a PWM array voltage waveform can be reconstructed using the Eq. 5 as well as PWM array current using the Eq. 10. For this purpose, Matlab has been used to generate the reconstructed PWM array voltage and current waveform, Figure 11.

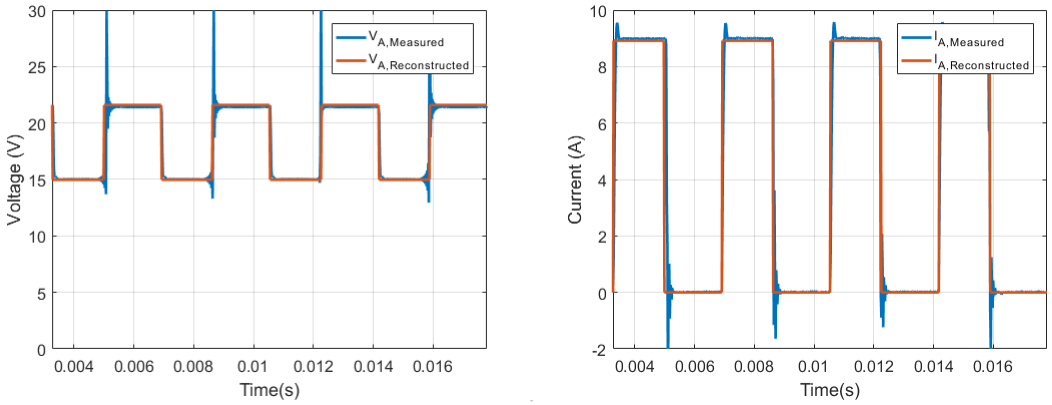


**a)** **b)**

*Figure 11 (a) Measured and Reconstructed PV array Voltage Waveform. (b) Measured and Reconstructed* PV array Current *Waveform* without any load.

As it has been shown, very sophisticated and expensive DAQ are needed when measuring at high frequency. Moreover, it is involved a huge amount of collected data. However, as it has been aforementioned, different ways are possible for implementing the proposed techniques which may use less complex and sophisticated DAQ together with true and average rms transducers. In addition, a sampling of one minute is allowed which will considerably reduce the data generated. The table below shows the comparison between "standard system" and the proposed system.

*Table 10* Features of monitoring systems in SAPV system with PWM charge regulator.

| | **DAQ features in order to monitor array PWM waveforms** | **DAQ features using the Proposed monitoring technique** |
|---|---|---|
| **Sampling mode** | Simultaneous channels are required for measuring array voltage and current. | Simultaneous channels are not required. A multiplexor could be used. |
| **Sampling frequency/ Sampling interval** The sampling frequency and sampling interval have been estimated with a PWM waveform which main frequency is 300Hz | 200 times the maximum frequency of the signal<br><br>200*300=60 kHz (2.77*$10^{-7}$ min) | <br><br>0.016 Hz (1 min) |
| **Storage capacity (approximated)** The storage capacity has been estimated with a PWM waveform which main frequency is 300Hz. | 1440*200*300=86400000 samples/day per monitoring parameter | 1440 samples/day per monitoring parameter |

ACCEPTED MANUSCRIPT

The techniques here developed provide affordable monitoring solutions of SAPV systems with PWM charge regulators which meet all the recommendations of IEC Standard 61724-1 as they achieve important pulse parameters such as high and low states of PWM waveforms together with its duty factor. From the latter it may be estimated the photovoltaic array DC power ($P_{A,DC}$), helping to detect array malfunctions. Accurate measurements of $P_{A,DC}$ manage to estimate properly not only the PV array DC output energy, $E_A$, but other calculated parameters such as the PV array energy yield, $Y_A$, and final system yield, $Y_F$. The latter indicate actual array operation relative to its rated capacity, $P_0$, and they are used as indicators of the performance of this type of systems.

Furthermore, at present, the different losses in a PV system specified by the IEC-61724 are only classified in two groups (i.e. system losses and capture losses). This classification does not properly discriminate the different types of losses that can occur in a SAPV system, making not easy the identification of possible malfunctions and delaying their solution. Using $P_{A,DC}$ and the duty factor obtained by the aforementioned monitoring method it can be estimated battery losses due to a high SOC during charge regulation in SAPV systems. The latter are structural losses of SPAV systems, and may easily mask other losses that are caused by SAPV system malfunctions. If they are quantified, it may be easy not only detect system malfunctions but to estimate other types of capture losses. In this sense, it may be improved the performance analysis of SAPV systems.

## 6. Conclusions

In this paper, a new and simple monitoring technique for stand-alone photovoltaic systems has been developed which can estimate the signals provided by the PWM battery charge controller, thus avoiding expensive DASs. As has been indicated in the previous sections, the International Standard IIEC Standard 61724-1 provides solutions that may not take into account the idiosyncrasy of SAPV systems with PWM BCC systems and batteries as the storage element. The sampling frequency, the large amount of data collected, the delay between channels for calculated parameters and the cost of DAS constitute relevant aspects to be considered when designing a system to monitor an SAPV system that uses a PWM battery charge controller. Although advanced and sophisticated DASs can measure PWM signals at high frequencies and provide simultaneous measurements of current, voltage or even $d_f$, this solution may be disproportionate considering the relatively low cost of the systems to be monitored.

An SAPV system with a series PWM battery charge controller, which is installed in the roof of Polytechnic School of University of Jaén, has been monitored under real conditions with advanced DAS measure PWM signals at the proper sampling frequency, which is in full compliance with the Annex A of the IEC 61724-1. The monitored data have been used to validate the developed technique to monitor PWM signals in SAPV systems using a sampling frequency of one minute and avoiding the complex DASs that require high sampling frequency, simultaneous sampling and huge data to process and analyse in order to measure the PWM current and voltage signals. The proposed technique can estimate the $d_f$ and the low and high state parameters of the current and voltage PWM waveform through measurements such as the average and the true root mean square values. Moreover, if the frequency is known or measured, the PWM waveform is easily estimated. It should be stated that PWM signal frequency is a fixed value given by a determined BCC.

Application software has been developed in LabVIEW to collect electrical and ambient parameters, to display and to store the data. On the other hand, the applications developed by Matlab have been employed for processing the measured data. As a result, the main electrical parameters, such as $d_f$, $I_{AP}$, $V_{oc}$, $V_{SL}$ show high accuracy with a mean absolute percentage error lower than 1.4%, a mean relative error within 1.4% and the coefficient of determination higher than 0.9. In accordance with the results obtained, the new technique presented can be used to calculate the key electrical parameters of current and voltage PWM waveforms of a PV array in stand-alone systems with series PWM battery charge controllers and, in this sense, estimate this type of waveforms. Moreover, the proposed technique may easily be extrapolated in order to estimate the PWM signals used in other applications where these types of signals are used.

ACCEPTED MANUSCRIPT

**ACKNOWLEDGEMENTS**

This research was funded by the Agencia Estatal de Investigación (AEI) and the Fondo Europeo de Desarrollo Regional (FEDER) aimed at the Challenges of Society (Grant No. ENE 2017-83860-R "Nuevos servicios de red para microredes renovables inteligentes. Contribución a la generación distribuida residencial"). The authors wish to thank the University of Jaén for the programme: "Plan de Apoyo a la I+D+I 2014-2015. Prorrogado hasta 2016". We also would like to acknowledge anonymous reviewers for their kind and interesting comments that have helped us to improve the manuscript.

References:

[1] EUROPEAN COMMISSION, Energy 2020. A strategy for competitive, sustainable and secure energy, Commun. FROM Comm. TO Eur. Parliam. Counc. Eur. Econ. Soc. Comm. Comm. Reg. (2010) 21. doi:COM(2010) 639.

[2] F. Nieuwenhout, M. Vervaart, P. van der Rijt, Monitoring of solar home systems in China: first year results, Energy. (2001) 1–4.

[3] B.S. Reddy, P. Balachandra, H.S.K. Nathan, Universalization of access to modern energy services in Indian households-Economic and policy analysis, Energy Policy. 37 (2009) 4645–4657. doi:10.1016/j.enpol.2009.06.021.

[4] M. Bazilian, P. Nussbaumer, C. Eibs-Singer, A. Brew-Hammond, V. Modi, B. Sovacool, V. Ramana, P.K. Aqrawi, Improving Access to Modern Energy Services: Insights from Case Studies, Electr. J. 25 (2012) 93–114. doi:10.1016/j.tej.2012.01.007.

[5] G. Almonacid, F.J. Muñoz, J. de la Casa, J.D. Aguilar, Integration of PV systems on health emergency vehicles. FIVE project, Prog. Photovoltaics. 12 (2004) 609–621. doi:10.1002/pip.558.

[6] X. Lemaire, Fee-for-service companies for rural electrification with photovoltaic systems : The case of Zambia, Energy Sustain. Dev. 13 (2009) 18–23. doi:10.1016/j.esd.2009.01.001.

[7] D. Palit, A. Chaurey, Off-grid rural electrification experiences from South Asia : Status and best practices, Energy Sustain. Dev. 15 (2011) 266–276. doi:10.1016/j.esd.2011.07.004.

[8] IRENA (International Renewable Energy Agency), REthinking Energy 2017: Accelerating the global energy transformation, Irena, Abu Dhabi, 2017.

[9] S. Sen, S. Ganguly, Opportunities, barriers and issues with renewable energy development -A discussion, Renew. Sustain. Energy Rev. 69 (2017) 1170–1181. doi:10.1016/j.rser.2016.09.137.

[10] International Renewable Energy Agency, Off-Grid Renewable Energy Systems: Status and Methodological Issues, Irena. Int. Renew. Energy Agency. (2015). http://www.irena.org/DocumentDownloads/Publications/IRENA_Off-grid_Renewable_Systems_WP_2015.pdf.

[11] D.P. Kaundinya, P. Balachandra, N.H. Ravindranath, Grid-connected versus stand-alone energy systems for decentralized power-A review of literature, Renew. Sustain. Energy Rev. 13 (2009) 2041–2050. doi:10.1016/j.rser.2009.02.002.

[12] V. Salas, E. Olías, A. Barrado, A. Lázaro, Review of the maximum power point tracking algorithms for stand-alone photovoltaic systems, Sol. Energy Mater. Sol. Cells. 90 (2006) 1555–1578. doi:10.1016/j.solmat.2005.10.023.

[13] I. Orlandi, N. Tyabji, J. Chase, M. Wilshire, B. Vickers, Off-grid solar market trends report 2016, (2016) 1–86. doi:10.1017/CBO9781107415324.004.

ACCEPTED MANUSCRIPT

[14] R. Khalilpour, A. Vassallo, Leaving the grid: An ambition or a real choice?, Energy Policy. 82 (2015) 207–221. doi:10.1016/j.enpol.2015.03.005.

[15] S. Daliento, A. Chouder, P. Guerriero, A.M. Pavan, A. Mellit, R. Moeini, P. Tricoli, Monitoring, diagnosis, and power forecasting for photovoltaic fields: A review, Int. J. Photoenergy. 2017 (2017). doi:10.1155/2017/1356851.

[16] K. Kalaitzakis, E. Koutroulis, V. Vlachos, Development of a data acquisition system for remote monitoring of renewable energy systems, Meas. J. Int. Meas. Confed. 34 (2003) 75–83. doi:10.1016/S0263-2241(03)00025-3.

[17] H. Rezk, I. Tyukhov, M. Al-Dhaifallah, A. Tikhonov, Performance of data acquisition system for monitoring PV system parameters, Meas. J. Int. Meas. Confed. 104 (2017) 204–211. doi:10.1016/j.measurement.2017.02.050.

[18] F.J. Muñoz, M. Torres, V. Muñoz, M. Fuentes, Monitoring Array Output Current and Voltage in Stand Alone Photovoltaics Systems With Pulse Width Modulated Charge Regulators, J. Sol. Energy Eng. 135 (2013). doi:10.1115/1.4007939.

[19] O. Kebour, A. Hadj Arab, A. Hamid, K. Abdeladim, Contribution to the analysis of a stand-alone photovoltaic system in a desert environment, Sol. Energy. 151 (2017) 68–81. doi:10.1016/j.solener.2017.05.009.

[20] IRENA, Accelerating off-grid renewable energy: IOREC 2014: Key findings and recommendations, Int. Off-Grid Renew. Energy Conf. Exhib. 2 (2014). http://www.irena.org/DocumentDownloads/Publications/IRENA_2nd_IOREC_2015.pdf .

[21] F.D.J. Nieuwenhout, A. Van Dijk, P.E. Lasschuit, G. Van Roekel, V.A.P. Van Dijk, D. Hirsch, H. Arriaza, M. Hankins, B.D. Sharma, H. Wade, Experience with solar home systems in developing countries: A review, Prog. Photovoltaics Res. Appl. 9 (2001) 455–474. doi:10.1002/pip.392.

[22] N.J. Williams, E.E. van Dyk, F.J. Vorster, Monitoring Solar Home Systems With Pulse Width Modulation Charge Control, J. Sol. Energy Eng. 133 (2011) 021006. doi:10.1115/1.4003586.

[23] IEEE Instrumentation and Measurement Society, IEEE Standard for Transitions , Pulses , and Related Waveforms, 2011. doi:10.1109/IEEESTD.2003.94394.

[24] F.J. Muñoz, G. Almonacid, G. Nofuentes, F. Almonacid, A new method based on charge parameters to analyse the performance of stand-alone photovoltaic systems, Sol. Energy Mater. Sol. Cells. 90 (2006) 1750–1763. doi:10.1016/j.solmat.2005.10.020.

[25] IEC, IEC 61724-1 Edition 1.0 2017-03 Photovoltaic system performance – Part 1: Monitoring IEC, Edition 1., IEC publications, Geneva, 2017.

[26] L.R. Chen, A design of an optimal battery pulse charge system by frequency-varied technique, IEEE Trans. Ind. Electron. 54 (2007) 398–405. doi:10.1109/TIE.2006.888796.

[27] A.N.S. Institute, IEEE Recommended Practice for Testing the Performance of Stand-Alone Photovoltaic Systems, 2001 (2001).

[28] International Energy Agency, Guidelines for Monitoring Stand-Alone Photovoltaic Power Systems - Methodology and Equipment, October. (2003).

[29] F.J. Muñoz, I. Echbarthi, G. Nofuentes, M. Fuentes, J. Aguilera, Estimation of the potential array output charge in the performance analysis of stand-alone photovoltaic systems without MPPT (Case study: Mediterranean climate), Sol. Energy. 83 (2009)

ACCEPTED MANUSCRIPT

1985–1997. doi:10.1016/j.solener.2009.07.012.

[30] R. Lara, R. Jimenez-Romero, F. Perez-Hidalgo, M.D. Redel-Macias, Influence of constructive parameters and power signals on sound quality and airborne noise radiated by inverter-fed induction motors, Meas. J. Int. Meas. Confed. 73 (2015) 503–514. doi:10.1016/j.measurement.2015.05.049.

[31] M.H. Chang, D. Das, P. V. Varde, M. Pecht, Light emitting diodes reliability review, Microelectron. Reliab. 52 (2012) 762–782. doi:10.1016/j.microrel.2011.07.063.

[32] Y. Hu, M.M. Jovanovic, LED driver with self-adaptive drive voltage, IEEE Trans. Power Electron. 23 (2008) 3116–3125. doi:10.1109/TPEL.2008.2004558.

[33] Microchip, Various Solutions for Calculating a Pulse and Duty Cycle, (2012) 1–22.

[34] Atmel, AVR135 : Using Timer Capture to Measure PWM Duty Cycle Table of Contents, (n.d.) 1–20.

[35] NI, Various ADC Types Used in NI DAQ Devices, (n.d.). https://knowledge.ni.com/KnowledgeArticleDetails?id=kA00Z0000019Nw5SAE (accessed September 17, 2018).

[36] NI, Calculating Absolute Accuracy or System Accuracy - National Instruments, (n.d.). http://www.ni.com/product-documentation/54387/en/#toc5 (accessed October 5, 2018).

[37] NI, DATASHEET. NI 9229, n.d. http://www.ni.com/pdf/manuals/374184c_02.pdf (accessed October 5, 2018).

[38] NI, DATASHEET. NI 9205, n.d. http://www.ni.com/pdf/manuals/378020a_02.pdf (accessed October 7, 2018).

[39] NI, DATASHEET. NI 9217, n.d. http://www.ni.com/pdf/manuals/374187a_02.pdf (accessed October 7, 2018).

[40] JCGM/WG 1, Evaluation of measurement data — Guide to the expression of uncertainty in measurement, GUM. 50 (2008) 134. doi:10.1373/clinchem.2003.030528.

[41] D. Grimaldi, M. Marinov, Distributed measurement systems, Meas. J. Int. Meas. Confed. 30 (2001) 279–287. doi:10.1016/S0263-2241(01)00019-7.

[42] Z.Y. Sheng, Realization of the motor data acquisition and analyzation system based on the producer/consumer model of LabVIEW, Proc. 2016 IEEE Adv. Inf. Manag. Commun. Electron. Autom. Control Conf. IMCEC 2016. (2017) 330–334. doi:10.1109/IMCEC.2016.7867227.

ACCEPTED MANUSCRIPT

ACCEPTED MANUSCRIPT

Highlights

- New monitoring technique for Stand-Alone Photovoltaic systems with PWM controllers.
- Estimation of duty factor, ‘low’ and ‘high’ states of PWM waveforms.
- The techniques may be used in other applications where PWM signals are used.

ACCEPTED MANUSCRIPT